Taylor & Francis
Taylor & Francis Group

Journal of Macromolecular Science, Part A
Pure and Applied Chemistry

ISSN: 1060-1325 (Print) 1520-5738 (Online) Journal homepage: http://www.tandfonline.com/loi/lmsa20

Fabrication of new polypyrrole/silicon nitride hybrid materials for potential applications in electrochemical sensors: Synthesis and characterization

Faiza Nessark, Ahmed Zouaoui, Alvaro Garcia-Cruz, Anne Bonhomme, Michael Lee, Belkacem Nessark, Nadia Zine, Pedro Marote, Joan Bausells, Abdoullatif Baraket & Abdelhamid Errachid

To cite this article: Faiza Nessark, Ahmed Zouaoui, Alvaro Garcia-Cruz, Anne Bonhomme, Michael Lee, Belkacem Nessark, Nadia Zine, Pedro Marote, Joan Bausells, Abdoullatif Baraket & Abdelhamid Errachid (2017) Fabrication of new polypyrrole/silicon nitride hybrid materials for potential applications in electrochemical sensors: Synthesis and characterization, Journal of Macromolecular Science, Part A, 54:11, 827-834, DOI: 10.1080/10601325.2017.1336728

To link to this article: http://dx.doi.org/10.1080/10601325.2017.1336728

Published online: 31 Jul 2017.

JOURNAL OF MACROMOLECULAR SCIENCE, PART A: PURE AND APPLIED CHEMISTRY
2017, VOL. 54, NO. 11, 827–834
https://doi.org/10.1080/10601325.2017.1336728

Fabrication of new polypyrrole/silicon nitride hybrid materials for potential applications in electrochemical sensors: Synthesis and characterization

Faiza Nessark[a,b], Ahmed Zouaoui[c], Alvaro Garcia-Cruz[a], Anne Bonhomme[a], Michael Lee[a], Belkacem Nessark[b], Nadia Zine[a], Pedro Marote[a], Joan Bausells[d], Abdoullatif Baraket[a] and Abdelhamid Errachid[a]

[a]Institut des Sciences Analytiques (ISA), Université Claude Bernard Lyon 1, 5 rue de la Doua, Villeurbanne cedex, France; [b]Laboratoire d'Electrochimie et Matériaux (LEM), Université Ferhat Abbas Sétif 1, Algeria; [c]Laboratoire de Croissance et Caractérisation de Nouveaux Semi-conducteurs (LCCNS), Université Ferhat Abbas Sétif 1, Algeria; [d]Centro Nacional de Microelectrónica (CNM), Universidad Autónoma de Barcelona, Bellaterra, Spain

ABSTRACT

In this research, an efficient fabrication process of conducting polypyrrole (PPy)/silicon nitride (Si_3N_4) hybrid materials were developed in order to be employed as transducers in electrochemical sensors used in various environmental and biomedical applications. The fabrication process was assisted by oxidative polymerization of pyrrole (Py) monomer on the surface of $Si/SiO_2/Si_3N_4$ substrate in presence of $FeCl_3$ as oxidant. To improve the adhesion of PPy layer to Si_3N_4 surface, a pyrrole-silane (SPy) was chemically bonded through silanization process onto the Si_3N_4 surface before deposition of PPy layer. After Py polymerization, $Si/SiO_2/Si_3N_4$-(SPy-PPy) substrate was formed. The influence of SPy concentration and temperature of silanization process on chemical composition and surface morphology of the prepared $Si/SiO_2/Si_3N_4$-(SPy-PPy) substrates was studied by FTIR and SEM. In addition, the electrical properties of the prepared substrates were characterized by cyclic voltammetry (CV) and electrochemical impedance spectroscopy (EIS). It was found that the best silanization reaction conditions to get $Si/SiO_2/Si_3N_4$-(SPy-PPy) substrate with high PPy adhesion and good electrical conductivity were obtained by using SPy at low concentration (4.3 mM) at 90°C. These promising findings open the way for fabrication of new hybrid materials which can be used as transducers in miniaturized sensing devices for various environmental and biomedical applications.

ARTICLE HISTORY
Received March 2017,
Revised and Accepted
May 2017

KEYWORDS
Silicon nitride; Polypyrrole; Oxidative polymerization; Surface characterization; Cyclic voltammetry; Electrochemical impedance spectroscopy

1. Introduction

Silicon nitride (Si_3N_4) plays an important role in microelectronics, integrated circuits technology, memory and thin film transistors, optoelectronics, optics, and hard surface coating (1, 2). Si_3N_4 offers a number of advantages when compared to other materials, such as the absence of undesirable impurities and the excellent control of the film composition and thickness (3). In addition, Si_3N_4 is considered as a biocompatible material in contact with bone *in-vitro* and it has been suggested as a load-bearing implant material due to its favorable mechanical properties (4). Also, the application of Si_3N_4 thick film for the fabrication and development of novel biosensors have been reported (5, 6). However, only few Si_3N_4-based biosensors have been successfully developed. This is due to the lack of an efficient and direct protocol for the integration of biological elements with Si_3N_4-based substrates and it is still one of its main drawbacks.

Nowadays, there is a great challenge to develop Si_3N_4 based devices. In this regard, the application of conductive polymers (CPs) has opened a new alternative to easily modify the Si_3N_4 substrate and to generate new materials with novel properties. Among all CPs, polypyrrole (PPy) is one of the most successfully employed polymers due to its high electrical conductivity, good environmental stability, biocompatibility, electro activity in neutral environments, and easy synthesis (7). PPy presents good electrical and optical properties for biosensor technology due to its π-electron conjugation along the polymer backbone (8, 9). Therefore, to enhance the conducting properties of Si_3N_4 semiconducting-based materials, recent studies have focused on the use of PPy conducting polymers as tools (transducers) which have the ability for amplification of the response signal arise from biomolecules interactions (e.g. in DNA biosensors, glucose sensing electrodes, amperometric enzyme biosensors, amperometric cholesterol biosensors, etc) (10–13).

Recently, Si_3N_4 and PPy have been used to generate novel Si_3N_4-PPy composites by using different techniques. For example, Si_3N_4 nanoparticles have been coated with PPy by the sonoelectrochemical synthesis of PPy (14). Besides, other techniques including the electrochemical grafting of PPy on porous silicon (Si) was used for gas sensors applications (15). Previously, we have reported PPy microstructures printed on glass and polyethylene terephthalate (PET) substrates for biosensing applications (16).

CONTACT Faiza Nessark faiza_nessark@yahoo.fr Institut des Sciences Analytiques (ISA), Laboratoire d'Electrochimie et Matériaux (LEM) Université Claude Bernard Lyon 1, 5 rue de la Doua, 69100 Villeurbanne cedex, France; Abdelhamid Errachid abdelhamid.errachid@univ-lyon1.fr Institut des Sciences Analytiques (ISA), Université Claude Bernard Lyon 1, 5 rue de la Doua, 69100 Villeurbanne cedex, France.

Color versions of one or more of the figures in the article can be found online at www.tandfonline.com/lmsa.

In this paper, we present a new technology to chemically synthesize Si/SiO_2/Si_3N_4-(SPy-PPy) hybrid materials that provide unique thermal, mechanical and electrical properties and could be employed for transducers in miniaturized sensing devices for various environmental and biomedical applications. This technique depends on chemical grafting of SPy on the activated Si/SiO_2/Si_3N_4 surface, followed by PPy deposition via oxidative polymerization of Py monomer. Factors affecting the properties of the prepared substrates were also studied including the concentration of silanizing agent (SPy) and the silanization reaction temperature, at which chemical grafting of SPy occurs at room temperature (r.t.) and at 90°C. Chemical structure and morphology of the prepared substrates were characterized at both temperatures using Fourier-transform infrared spectroscopy (FTIR) and scanning electron microscopy (SEM). In addition, the electrical properties of the resulting Si/SiO_2/Si_3N_4-(SPy-PPy) substrates were measured by cyclic voltammetry (CV) and electrochemical impedance spectroscopy (EIS).

2. Materials and equipment

2.1. Materials

N-(3-trimethoxysilylpropyl)pyrrole ($C_{10}H_{19}NO_3Si$) or SPy was purchased from ABCR GmbH & Co. KG, Germany. Chloroform ($CHCl_3$) was purchased from Fisher Scientific, France. Sulfuric acid (H_2SO_4) (30%), hydrochloric acid (HCl) (37%), sodium dodecyl sulphate ($C_{12}H_{25}NaO_4S$) or SDS, iron (III) chloride ($FeCl_3$), methanol (CH_3OH), acetone (C_3H_6O), and pyrrole (C_4H_5N) (98%) were purchased from Sigma-Aldrich, France. Hydrogen peroxide (H_2O_2) (35% wt.), sodium hydroxide (NaOH), and phosphate buffer saline (PBS) (pH 7.4) were obtained from Acros Organics, France. Uniform chips (1.2 × 1.2 cm^2) of the basic sensor substrate material [Si/SiO_2/Si_3N_4] were used in this study.

2.2. Equipment

2.2.1. FTIR spectroscopy

Chemical composition of the prepared substrates before and after polypyrrole deposition was identified by infrared (IR) spectroscopy analysis using Fourier-transform infrared spectroscopy (FTIR) spectrometer model NEXUS (Nicolet-Thermo Fisher, UK). The spectra were recorded in attenuated total reflectance (ATR) mode with a Thunderdome (Spectra-tech) accessory containing Germanium crystal with a mono reflection at 45°. A DTGS detector was employed with 4 cm^{-1} resolution and Happ-Genzel Apodization at 256 scans.

2.2.2. Electronic microscopy

Morphology of the deposited polypyrrole layer of the prepared Si/SiO_2/Si_3N_4-(SPy-PPy) hybrid substrates was examined using scanning electron microscope (SEM), FEI Quanta 250 FEG, France.

2.2.3. Electrochemical experiments

The conductivity of the prepared Si/SiO_2/Si_3N_4-(SPy-PPy) substrates was evaluated by electrochemical measurements consisting of EIS and CV using a potentiostat/galvanostat Auto Lab (EC-lab VMP3 instruments version 9.9), Bio-Logic-Science Instruments, France. The controlling software (EC-Lab V10.39, 2014) was used for modeling and fitting the impedance data. The experiments were achieved in a miniaturized electrochemical plastic cell (Ø = 0.503 cm^2, active area) with a three electrodes system. Here, the Si/SiO_2/Si_3N_4-(SPy-PPy) substrate was applied as the working electrode (WE), a platinum wire was applied as the counter electrode (CE), and a saturated calomel electrode (SCE) was used as the reference electrode (RE). A freshly prepared PBS (200 μL at 10 mM, pH 7.4) solution was employed for all analyses as the electrolyte solution. The CV experiments were performed at a potential between −0.8 and +0.5 V/SCE with scanning rate 25 mV/s. The EIS parameters for the potential, sinus amplitude, and frequency range, were adjusted at −0.1 V/SCE, 25 mV, and 100 kHz to 50 mHz, respectively. For the Nyquist plot fitting, the randomize + simplex method was used with randomize stopped on 10000 iterations and the fitting was stopped on 5000 iterations.

3. Production of Si/SiO_2/Si_3N_4-(SPy-PPy) substrates

3.1. Fabrication of Si/SiO_2/Si_3N_4 substrate

The structure of Si/SiO_2/Si_3N_4 sensor substrate used in this study was fabricated according to standard microelectronic technology with a p-type <100> silicon wafer doped with Boron (17). Silicon dioxide (SiO_2) layer (1000 Å) was thermally grown. Afterwards, a layer (1000 Å) of Si_3N_4 was deposited by low-pressure chemical vapor deposition (LPCVD) technique (18). Finally, the prepared Si/SiO_2/Si_3N_4 substrates were rinsed thoroughly and sonicated in deionized water for 20 min. Uniform chips (1.2 × 1.2 cm^2) of the Si/SiO_2/Si_3N_4 were prepared as the basic sensor substrate material used in this study.

3.2. Substrate cleaning and activation process

Before silanization process, Si/SiO_2/Si_3N_4 substrates were cleaned with acetone using ultrasonication (15 min, twice), then rinsed with ultra-pure water and finally dried under Nitrogen flow. After that the substrates were treated with a piranha solution (3:1 V/V, H_2SO_4:H_2O_2) at 90°C for 30 min, followed by thoroughly rinsing with ultra-pure water. The substrates were then subjected to successive alkaline and acidic treatments as follow: 1) Treatment with NaOH (0.5 M) aqueous solution for 20 min, followed by rinsing with ultra-pure water. 2) Treatment with HCl (0.1 M) solution for 10 min, and therinsing with ultra-pure water. 3) Alkali treatment with NaOH (0.5 M) for 10 min. Finally, the samples were rinsed thoroughly with HCl (0.1 M) and ultra-pure water and then dried in an oven at 120°C for 10 min (19). All above mentioned treatments allow to create active sites (–OH reactive groups) on the Si/SiO_2/Si_3N_4 substrate surface (Scheme 1(a)).

3.3. Si/SiO_2/Si_3N_4 substrate silanization process

After activation process, the activated substrates (Si/SiO_2/Si_3N_4-OH) were silanized with SPy at different concentrations (4.3 mM, 21.5 mM, 43 mM, and 107.5 mM) in $CHCl_3$ anhydrous by depositing a drop of the solution onto the Si_3N_4 surface. The

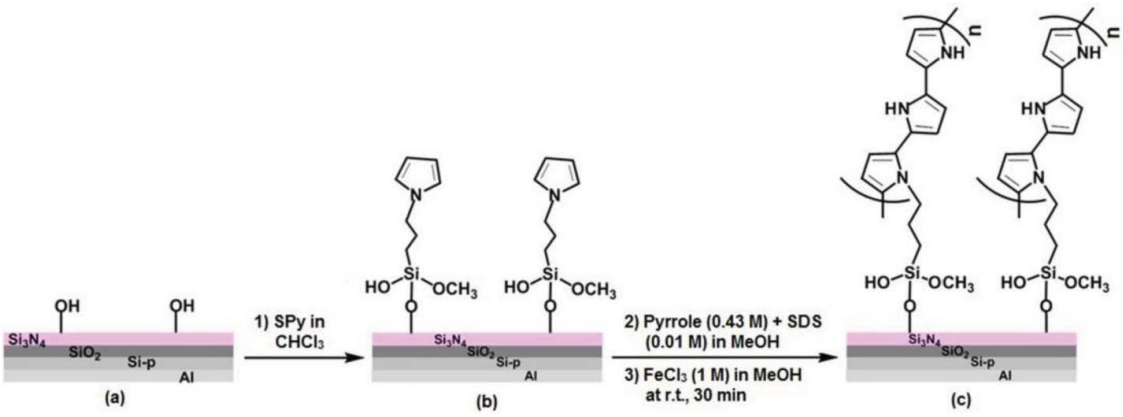

Scheme 1. Schematic procedure for fabrication of $Si/SiO_2/Si_3N_4$-(SPy-PPy) substrate via: (a) activation of $Si/SiO_2/Si_3N_4$ substrate, (b) silanization of substrate by SPy forming ($Si/SiO_2/Si_3N_4$-SPy) substrate and (c) development of $Si/SiO_2/Si_3N_4$-(SPy-PPy) substrate via polypyrrole layer deposition through oxidative polymerization of Py monomer on the silanized substrate.

anhydrous solvent and dehydrated materials promote the formation of a very dense SPy monolayer (20, 21). After SPy deposition, the substrates were divided into two groups and silanization reaction was left to proceed for 1 hour at room temperature (r.t.) till the complete evaporation of solvent (group 1) and at 90°C for 1 h (group 2). The functionalization of $Si/SiO_2/Si_3N_4$ substrates with SPy is represented in Scheme 1(b). Here, the SPy molecules were covalently bonded to the $Si/SiO_2/Si_3N_4$ substrate via condensation reaction with the hydroxyl (–OH) groups on the activated silica surface forming Si–O–Si link. After silanization process, the substrates were rinsed several times with chloroform in order to remove unreacted SPy molecules, and then left to dry at room temperature.

3.4. Chemical deposition of PPy layer via oxidative Py polymerization

After silanization process, all silanized substrates ($Si/SiO_2/Si_3N_4$-SPy) were modified by adding 50 μL of a solution containing a mixture of Py monomer (0.43 M) and SDS (0.01 M) stabilizing agent in methanol. This solvent has been reported as the best solvent used for preparation of PPy with high conductivity (190 S/cm) by chemical polymerization (18, 19). Subsequently, the oxidative polymerization of Py was performed by the addition of 50 μL of $FeCl_3$ (1 M) in methanol at r.t. for 30 min. The molar ratio of pyrrole monomer to the oxidant (Py: $FeCl_3$) was employed at 1:2.33 (9, 22, 23). Then, the polymerization of SPy anchoring monomer with the Py monomer was started simultaneously by addition of $FeCl_3$ oxidant to produce $Si/SiO_2/Si_3N_4$-(SPy-PPy) hybrid material, as shown in Scheme 1(c). After polymerization, the substrates were rinsed several times with methanol to remove the hydrated $FeCl_3$, and unreacted Py monomer, and then dried in an oven at 50°C for 12 h.

4. Results and discussion

4.1. Characterization of $Si/SiO_2/Si_3N_4$-(SPy-PPy) substrates by FTIR

After cleaning and activation processes, FTIR spectra of the $Si/SiO_2/Si_3N_4$ surface were examined. As clearly seen from Fig. 1, the FTIR spectra of $Si/SiO_2/Si_3N_4$ before and after activation showed intense bands between 1200 cm^{-1} and 800 cm^{-1} due to Si–O and Si–N bonds of the substrate, respectively. In addition, a slightly broad band at 3200- 3400 cm^{-1} appeared for activated substrate, suggesting that Si_3N_4 surface is rapidly hydrolyzed to generate –OH groups on the substrate surface (24, 25).

The effect of SPy concentration and silanization temperature on the silanization process have been also studied using FTIR measurements (Fig. 1(A) and 1(B) for group 1 and group 2 respectively). The FTIR spectra of all SPy-modified substrates ($Si/SiO_2/Si_3N_4$-SPy) did not clearly show the typical Si–O–Si bands of Si–O–SPy due to the overlapping with the substrate signal, which generally appears in the region of 800–1200 cm^{-1}. Moreover, the SPy-modified substrates showed characteristic vibration bands of the SPy molecule at

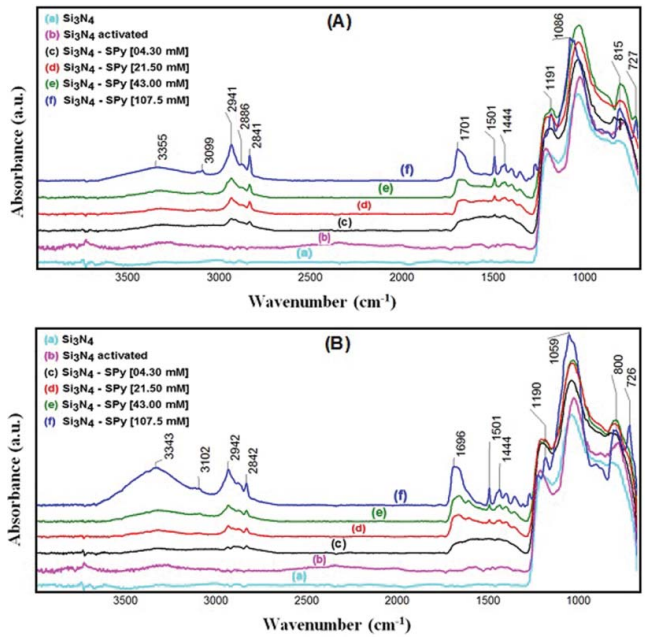

Figure 1. FTIR spectra of $Si/SiO_2/Si_3N_4$ substrates before and after activation, and after treatment with different molar concentrations of SPy at r.t. (group 1) (A), and at 90°C (group 2) (B).

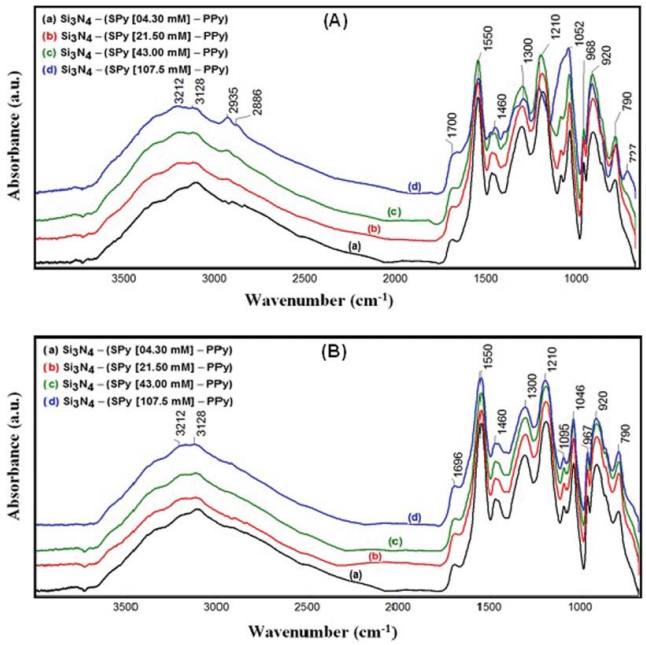

Figure 2. FTIR spectra of PPy layer deposited on the SPy-treated $Si/SiO_2/Si_3N_4$ substrates with different SPy molar concentrations at r.t. (group 1) (A), and at 90°C (group 2) (B).

1501 cm^{-1} and 1444 cm^{-1} which assigned to the C–C and C–N stretching vibration of pyrrole ring, respectively.

Other characteristic bands of SPy appeared at ≈3100 cm^{-1} due to C–H stretching vibration of pyrrole cycle (= C–H) (26), as well as between 2800 cm^{-1} and 3000 cm^{-1} which are related to the stretching vibrations of aliphatic $–CH_2$ and $–CH_3$ groups. At the highest SPy concentration (107.5 mM), the treated substrate showed a band at 1190 cm^{-1}that is characteristic to the deformation vibration of the CH_3 of $Si–O–CH_3$ and near to 1090 cm^{-1} for the asymmetric vibration of Si–O–C bond. In addition, abroad band at 3340–3350 cm^{-1} was visible for the SPy-treated substrate. This characteristic band is related to stretching vibration of the –OH group, suggesting the presence of silanol group Si–OH.

After pyrrole polymerization, the characteristic vibration bands of PPy deposited on the $Si/SiO_2/Si_3N_4$-SPy substrate were appeared, confirming the formation of $Si/SiO_2/Si_3N_4$-(SPy-PPy) hybrid substrate. As shown in Fig. 2 (A) and (B), the appearance of a broad peak near to 3200 cm^{-1} is assigned to the presence of N–H stretching vibrations. The deformation C–N bands at 1300 cm^{-1} and C–H on plane bending vibration at 1210 cm^{-1} were also observed (27, 28). Moreover, the peaks appeared at 3128 cm^{-1}, 1550 cm^{-1}, and 1460 cm^{-1} are attributed to the = C–H, C = C, and C–N vibrations of pyrrole cycle, respectively (28–30). In addition, the characteristic bands of PPy were observed at 920 cm^{-1} and at 790 cm^{-1} due to C–H ring out-of-plane bending mode (31, 32).

Moreover, a new band around 1700 cm^{-1} was also observed, which is related to the characteristic stretching vibration of carbonyl group (C = O). The arising of this group may be attributed to the reaction between the propagating pyrrole radical cations and water that lead to the termination or quenching of polymerization reaction (33–35), as shown in Scheme 2, or due to oxidation in the presence of oxygen and water during the drying process (27).

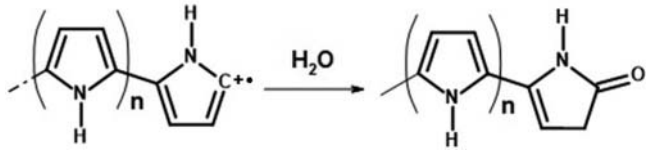

Scheme 2. Proposed scheme for termination of pyrrole polymerization via reaction of propagating PPy radical cation with water [29].

In fact, regardless of the SPy concentration or silanization temperature, the FTIR spectra analysis proved the successful silanization of Si_3N_4 surface and the effective chemical deposition of PPy layer, forming $Si/SiO_2/Si_3N_4$-(SPy-PPy) hybrid substrates.

4.2. SEM characterization

Morphology of the PPy layer deposited on $Si/SiO_2/Si_3N_4$-SPy substrates modified with different molar concentrations of SPy at 90°C was examined by SEM (Fig. 3). The SEM images clearly showed the successful deposition of PPy layer on $Si/SiO_2/Si_3N_4$-SPy substrate surface. The PPy layer was deposited in the form of grains or particles tangled with each other, forming a uniform porous structure. The size of these grains is ranged from 150 nm to 379 nm. Here, it is interesting to notice that the PPy layer deposited at low SPy concentration (4.3 mM) contains bridges with uniform geometric-like structure. By increasing the concentration of SPy progressively, the PPy grains were fused together. As a result, less porous and much denser PPy layers were obtained. Similarly, the SEM images of $Si/SiO_2/Si_3N_4$-(SPy-PPy) substrates silanized at room temperature showed the same morphology (results are not shown here).

These observations suggest that the PPy particles were covalently deposited on the SPy layer of the silanized substrates ($Si/SiO_2/Si_3N_4$-SPy) which significantly modified the final morphology of the PPy polymer. This was evidenced by the appearance of PPy particles which are relatively piled on a layer of SPy molecules. In addition, the uniform geometric-like structure of the PPy particles indicates that the SPy molecules under the PPy layer were uniformly distributed on the $Si/SiO_2/Si_3N_4$ substrate surface which contributes in the formation of PPy porous layer with high surface area. This in turn will improve the physicochemical properties of the prepared $Si/SiO_2/Si_3N_4$-(SPy-PPy) hybrid substrate such as chemical reactivity, electrical conductivity, etc., which are considered as basic requirements for electrochemical sensor devices.

4.3. Electrochemical characterization of the $Si/SiO_2/Si_3N_4$-(SPy-PPy) substrates

4.3.1. Cyclic voltammetry (CV) analysis

The prepared $Si/SiO_2/Si_3N_4$-(SPy-PPy) substrates modified with SPy at different concentrations and different temperatures (at room temperature (group1) and at 90°C (group2)) were characterized by CV in order to analyze the electrochemical behavior of the PPy layer. The potential range applied was between - 0.8 and + 0.5 V/SCE with a scan rate 25 mV/s. The

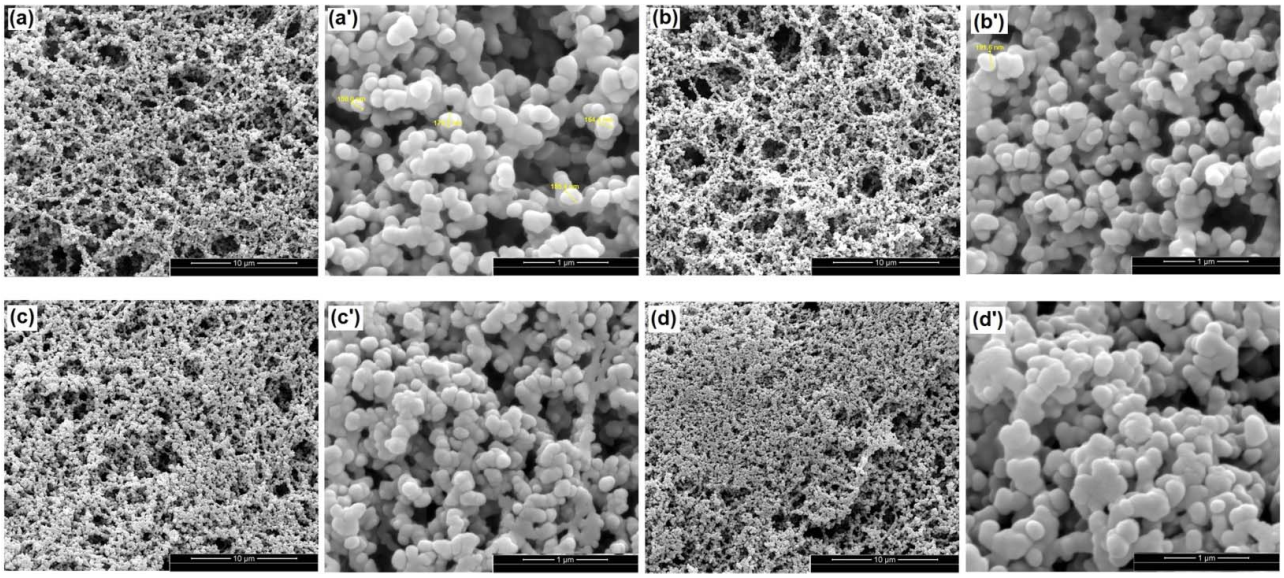

Figure 3. SEM images of PPy layer deposited on the $Si/SiO_2/Si_3N_4$ substrates-treated with SPy at different molar concentrations at 90°C: (a, a') 4.3 mM, (b, b') 21.5 mM, (c, c') 43 mM, and (d, d') 107.5 mM.

analysis of the PPy layer was carried out in a physiological electrolyte PBS buffer solution (pH 7.4), which is commonly used in biosensors applications because it is isotonic and non-toxic to most cells. As shown in the cyclic voltammograms (Fig. 4), no oxidation peaks were observed during scanning of the positive potential for both group 1 and group 2 substrates. Here, it is worth to mention that a strong capacitive current (I) was observed during the positive potential sweeps which may led to the disappearance of the PPy oxidation peak. This high capacitive current may be attributed to the high specific surface area of the porous PPy film deposited on the Si_3N_4 substrate, as evidenced by SEM measurements (Fig. 3). In some reaction cases the capacitive current contribution can be minimized by decreasing the scan rate. However, even at low scanning speed, the capacitive current remains high in the case of conductive polymers. Indeed, different phenomena of polarization can take place; such as, for example, concentration and resistance polarizations, due to the presence of the polymer film on the electrode, which make the diffusion of the electrolyte species on the surface and inside the film difficult. This in turn contributes to increasing the capacitive current, whereas the contribution of the Faradic current becomes negligible.

On the other hand, the characteristic PPy reduction peak at around -0.4 V/SCE was observed during scanning of the negative potentials. In addition, an increasing in the height (intensity) of the reduction peak, accompanied by a reduction peak displacement to more negative potential values, was noticed by increasing SPy concentration. The potential is a thermodynamic parameter; its slight displacement towards other negative values shows a slight modification in the physicochemical properties of the surface which takes place when the concentration of SPy increases. The latter becomes more and more negative when the rate of overlap of the surface by the molecules SPy increases. Indeed, these cyclic voltammograms are significantly inclined, more particularly in case of group 2 (SPy treatment at 90°C), and progressively by increasing SPy concentration.

4.3.2. Electrochemical impedance spectroscopy (EIS) measurements

EIS measurements of the $Si/SiO_2/Si_3N_4$-(SPy-PPy) hybrid substrate modified with different SPy concentrations at two different temperatures (group 1 and group 2) are represented in Fig. 5. The EIS analysis was performed in PBS physiological solution (pH 7.4) with an applied potential of - 0.1 V/SCE, a frequency range between 100 kHz and 50 mHz, and AC voltage of 25 mV. As shown in Fig. 5, the Nyquist impedance plots of the PPy films are measured as a function of SPy concentrations, where Re(Z) is the real part and Im(Z) is the imaginary part of the complex impedance Z. The Nyquist impedance plots are composed of two semi-circles at low SPy concentrations and a single arc at high SPy concentrations. The electrical properties depend on the nature and structure of the film formed on the electrode, which is dependent on the concentration of SPy. These semi-circle plots are characteristic for the charge transfers process though the PPy layer. The diameter of the semi-circles increases in parallel with the SPy concentration, indicating the increase of impedance or charge transfer resistance (R_{ct}), which in turn reduces the electrical conductivity of PPy layer by increasing SPy concentration. The presence of SPy layer at higher concentrations on the $Si/SiO_2/Si_3N_4$ substrate makes the substrate less conductive and consequently prevents or retards the electron transfer process. These results are in agreement with those obtained by Micusıket al (36).

Indeed, impedance diagram in the form of capacitive loops may well explain the strong contribution of capacitive current, as previously indicated in CV measurements by the inclined shape (ill-defined) and the by high capacitive current observed during the positive potential sweeps of CV (Fig. 4).

For more explanation of the electrochemical properties, the impedance spectra of $Si/SiO_2/Si_3N_4$-(SPy-PPy) substrates were analyzed by using the equivalent circuit's models, which are appropriate for conducting polymer films deposited on electrode surfaces, as described in the literature (37–39). Here it is worth to mention that impedance (Z) is a totally complex

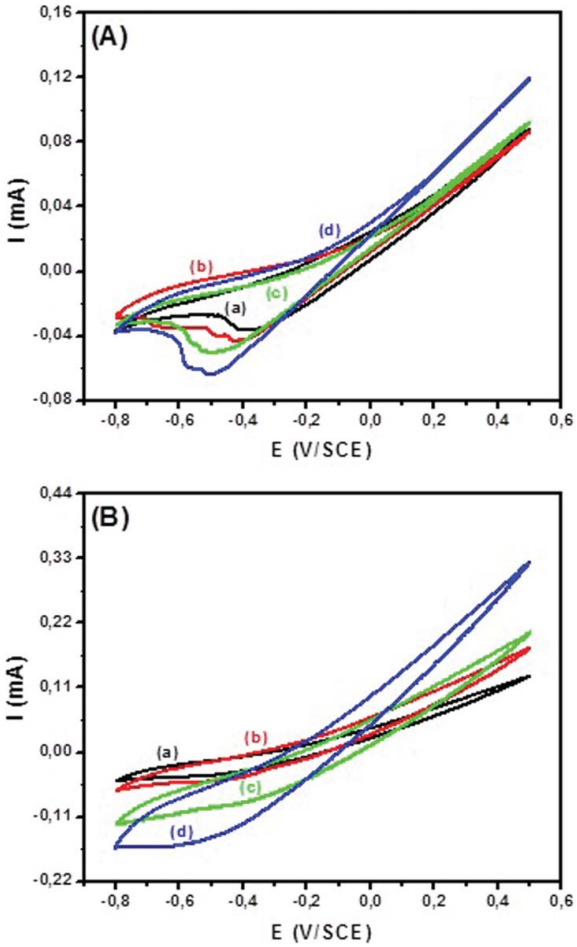

Figure 4. Cyclic voltammograms of PPy layer deposited on the SPy-modified Si/SiO_2/Si_3N_4 substrates at different SPy concentrations: (a) 4.3 mM, (b) 21.5 mM, (c) 43 mM, and (d) 107.5 mM, at r.t. (group1) (A), and at 90°C (group2) (B). (Scale bar for a, b, c, and d is 10 μm and for a′, b′, c′, and d′ is 1 μm).

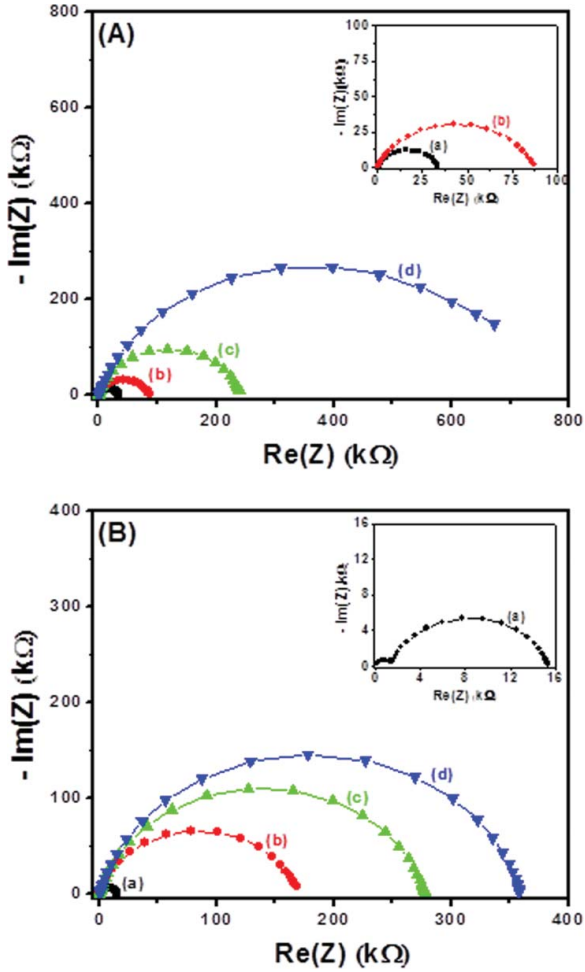

Figure 5. Nyquist plots of PPy layer deposited on the SPy-modified Si/SiO_2 /Si_3N_4 substrates at different SPy concentrations: (a) 4.3 mM, (b) 21.5 mM, (c) 43 mM, and (d) 107.5 mM, at r.t. (group1) (A), and at 90°C (group2) (B).

resistance encountered when a current flows through a circuit made of resistors, capacitors, or inductors, or any combination of these. Depending on how the electronic components are configured, both the magnitude and the phase shift ($\alpha.\pi/2$) of an alternating current (AC) can be determined. Because, the inductive effect is not usually encountered in electrochemistry, we consider only the simple equivalent circuit shown in Fig. 6 in which no inductor is present. In this equivalent circuit model, the various electrical parameters contributed in the electrical impedance measurements are represented as: solution resistance (R_s), capacitance of the polymer film (C_f), polymer film resistance (R_f), constant phase element (*CPE*), charge transfer resistance at the polymer film/electrolyte interface (R_{ct}), and Warburg impedance (*W*) which is created as a result of electrolyte species diffusion through the Nernst diffusion layer and can be also expressed by Warburg impedance (40).

The electrical parameters values obtained by fitting data, using the equivalent circuit depicted in Fig. 6, are summarized in Table 1. As clearly seen, all electrical parameters were obtained with very good fitting (i.e. with very low fitting correlation coefficient χ^2 values). In fact, this equivalent circuit allows the distinguishing between the intrinsic electrical characteristics related to C_f and R_f of the polymer film, which are related to the ionic charges mobility through the polymer backbone during the doping/dedoping process and to the charge transfer resistance (R_{ct}) at the polymer/electrolyte or electrode/polymer interfaces (41).

Concerning the charge transfer resistance R_{ct}, as clearly indicated in Table 1, the value of R_{ct} increases by increasing SPy concentration. This can be explained by the formation of a dense insulating layer of SPy which may prevents or impede the electronic charge transfer through the deposited PPy film or that result from other secondary physical phenomena. These include, for example, heterogeneous dispersion of charges which may arise from modification of the morphology and variation in the real surface area of PPy film, which depend on SPy concentration.

In general, it was found that the lowest R_{ct} values (i.e. the best conductivities) were obtained for the Si/SiO_2/Si_3N_4-(SPy-PPy) substrates treated with the lowest SPy concentration,

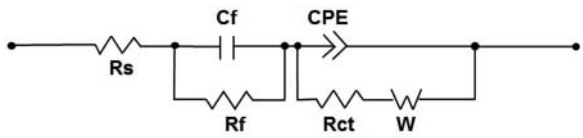

Figure 6. Equivalent electrical circuit model for Si/SiO_2/Si_3N_4-(SPy-PPy) substrates.

Table 1. Electrochemical parameters obtained from fitting of the experimental results of PPy layer deposited on the $Si/SiO_2/Si_3N_4$ substrates treated with different concentrations of SPy at room temperature (group 1), and at 90°C (group 2).

Group no.	C_{SPy} (mM)	R_s (Ω)	$C_f\ 10^{-9}$ (F)	R_f (Ω)	CPE 10^{-9} ($F.s^{(\alpha-1)}$)	α_{CPE}	$R_{ct}(\Omega)$	$W(\Omega.s^{-1/2})$	χ^2
Group 1 at room temp.	4.3	141	13.77	717.7	919.4	0.80	33190	22.32	0.07834
	21.5	109.8	11.53	465.4	162.5	0.78	86412	630.2	0.02213
	43.0	83.86	16.49	320.5	75.29	0.85	239164	2969	0.01298
	107.5	93.21	10.45	335.6	87.42	0.82	688077	83676	0.05840
Group 2 at 90°C	4.3	109.7	6.379	1276	835.1	0.84	13979	21.58	0.06894
	21.5	46.2	9.581	128.3	60.77	0.85	167430	4808	0.05030
	43.0	79.1	13.75	190.9	44.67	0.87	266372	5769	0.03616
	107.5	165.8	5.71	383.3	36.85	0.90	347700	7625	0.01727

C_{SPy} is the SPy concentration, α is phase shift coefficient and its value $= 0 < \alpha < 1$, W is Warburg diffusion resistance, and χ^2 is the fitting correlation coefficient.

weather at room temperature or at 90°C. However, at the lowest SPy concentration investigated, the R_{ct} values are relatively higher for group 1 substrates than those of group 2. This can be attributed to the effect of thermal treatment at 90°C during silanization process, which may lead to partial evaporation and consequently lowering in the concentration of SPy molecules on the surface of $Si/SiO_2/Si_3N_4$ substrate. Moreover, in case of group 2 substrates, upon successive increasing of SPy concentration, the R_{ct} values of $Si/SiO_2/Si_3N_4$-(SPy-PPy) substrate turned to be higher than those in group 1. In fact, at high temperature the reaction of SPy in excess amount with the activated substrate cannot be controlled. This phenomenon is common to all trialkoxysilanes (e.g. pyrrole-silane), namely, that polymerization can occur at the free SPy silanol group (Si-OH) on the surface or in solution prior to condensation with the solid substrate. This leads to a highly polymeric and heterogeneous surface or unreacted SPy molecules to the substrate surface, a potential disadvantage when preparing homogeneous surfaces for biosensing applications (42).

4. Conclusions

In the present research, an efficient synthetic method for elaborating conducting $Si/SiO_2/Si_3N_4$-(SPy-PPy) hybrid materials was reported. This method was assisted by activation and modification of the $Si/SiO_2/Si_3N_4$ semi-conducting substrate surface with pyrrole-silane (SPy) molecules, followed by chemical deposition of PPy conducting polymer layer via chemical oxidative polymerization of Py on the SPy-modified substrate. FTIR spectra showed the successful formation of $Si/SiO_2/Si_3N_4$-(SPy-PPy) substrates, as proved by the several characteristic bands of SPy and PPy on the surface of activated $Si/SiO_2/Si_3N_4$ substrate. In addition, SEM images showed the successful chemical deposition of PPy layer on $Si/SiO_2/Si_3N_4$-SPy substrate. Moreover, the structure, morphology and surface area of PPy conducting layer were significantly modified with the concentration of SPy grafted on $Si/SiO_2/Si_3N_4$ substrate.

More interestingly, SPy concentration and temperature of the silanization process played an important role for determining the conductivity of the prepared $Si/SiO_2/Si_3N_4$-(SPy-PPy) hybrid substrates. Based on CV and EIS measurements, the best conductivity was obtained for the $Si/SiO_2/Si_3N_4$-(SPy-PPy) hybrid substrates treated with the lowest SPy concentration (4.3 mM), in general, and more particularly at 90°C. Oppositely, by increasing the concentration of SPy, the PPy films obtained were more resistant (less conductive).

These preliminary results are promising and can be exploited for creating new conducting polymer hybrid materials with controlled electrochemical properties depending on the preparation conditions. In addition, they can be integrated as transducers (for amplification of the electrochemical signal response arising from the biomolecules interaction with PPy layer) in electrochemical sensors or in lab-on chip devices that have wide environmental and biomedical applications (e.g. biosensors).

Acknowledgements

We acknowledge the funding through the European Communities Seventh Framework Programme entitled Sea-on-a-Chip (FP7-OCEAN-2013) (No.614168), and the European Union's Horizon 2020 research and innovation program entitled HEARTEN under grant agreement No 643694, and FP7-PEOPLE-2012-IRSES under the grant agreement No. 318053 (SMARTCANCERSENS).

References

1. Custer, J. S., Smith, P. M., Fleming, J. G., Roherty-Osmun, E. (1999) ACS Symposium Series Inorganic Materials Synthesis, 86–99.
2. Joshi, B. C., Eranna, G., Runthala, D. P., Dixit, B. B., Wadhawan, O. P., Vyas, P. D. (2000) Indian J. Eng. Mater. S., 7: 303–309.
3. Caballero, D., Martinez, E., Bausells, J., Errachid, A., Samitier, J. (2012) Anal. Chim. Acta, 720: 43–48.
4. Gustavsson, J., Altankov, G., Errachid, A., Samitier, J., Planell, J. A., Engel, E. (2008) J. Mater. Sci-Mater. M., 19(4): 1839–1850.
5. Travas-Sejdic, J., Peng, H., Cooney, R., Bowmaker, G., Cannell, M., Soeller, C. (2006) Curr. Appl. Phys., 6: 562–566.
6. Choi, C. K., English, A. E., Jun, S.-I., Kihm, K. D., Rack, P. D. (2007) Biosen. Bioelectron., 22(11): 2585–2590.
7. Caballero, D., Samitier, J., Bausells, J., Errachid, A. (2009) Small, 5(13): 1531–1534.
8. Ates, M. (2013) Mater. Sci. Eng. C Mater. Biol. Appl., 33(4): 1853–1859.
9. Dridi, F., Marrakchi, M., Gargouri, M., Garcia-Cruz, A., Dzyadevych, S., Vocanson, F., Lagarde, F. (2015) Sensor. Actuat. B-Chem., 221: 480–490.
10. Garcia-Cruz, A., Lee, M., Zine, N., Sigaud, M., Bausells, J., Errachid, A. (2015) Sensor. Actuat. B-Chem., 221: 940–950.
11. Gursoy, S. S., (Gok), A. U., Tilki, T. (2010) J. Macromol. Sci. A, 47: 681–688.
12. Özer, B. O., Çete, S. (2016) Artif. Cells Nanomed. Biotechnol., 45: 824–832.
13. Guiseppi-Elie, A., Brahim, S., Narinesingh, D. (2001) J. Macromol. Sci. A, 38: 1575–1591.
14. Ashassi-Sorkhabi, H., Bagheri, R. (2014) Synthetic Met., 195: 1–8.

15. Tebizi-Tighilt, F.-Z., Zane, F., Belhaneche-Bensemra, N., Belhousse, S., Sam, S., Gabouze, N.-E. (2013) Appl. Surf. Sci., 269: 180–183.
16. Garcia-Cruz, A., Zine, N., Sigaud, M., Lee, M., Marote, P., Lanteri, P., Errachid, A. (2014) Microelectron. Eng., 121: 167–174.
17. Oliveira, I. A. M. D., Torrent−Burgués, J., Pla, M., Zine, N., Bausells, J., Escriche, L., Samitier, J. (2006) Anal. Lett., 39(8): 1709–1720.
18. Oliveira, I. M. D., Pla, M., Escriche, L., Casabo, J., Zine, N., Bausells, J., Errachid, A. (2004) Proc. IEEE Sensors.
19. Wei, Z., Wang, C., Bai, C. (2000) Surf. Sci., 467(1–3): 185–190.
20. Mutin, P. H., Guerrero, G., Vioux, A. (2005) J. Mater. Chem., 15(35–36): 3761.
21. Glaser, A., Foisner, J., Hoffmann, H., Friedbacher, G. (2004) Langmuir, 20(13): 5599–5604.
22. Machida, S., Miyata, S., Techagumpuch, A. (1989) Synth. Met., 31(3): 311–318.
23. Brezoi, D.-V. (2010) Am. j. sci. arts, 1: 53–58.
24. Bermudez, V. M. (2005) J. Electrochem. Soc., 152 (2): F31–F36.
25. Merlini, C., Rosa, B. S., Müller, D., Ecco, L. G., Ramôa, S. D., Barra, G. M. (2012) Polym. Test., 31(8): 971–977.
26. Łydżba-Kopczyńska, B., Beć, K., Tomczak, J., Hawranek, J. (2012) J. Mol. Liq., 172: 34–40.
27. Organic Electrochemistry-an Introduction and a Guide, 2nd Ed., Edited by Manuel M. Baizer, and Henning Lund (1983) Marcel Dekker, New York, p. 1166. J. Polymer Sci. Polymer Lett. Ed., 22 (1984) 459–459
28. Kasisomayajula, S. V., Qi, X., Vetter, C., Croes, K., Pavlacky, D., Gelling, V. J. (2009) J. Coat. Technol. Res., 7(2): 145–158.
29. Jadhav, N., Vetter, C. A., Gelling, V. J. (2013) Electrochim. Acta, 102: 28–43.
30. Chougule, M. A., Pawar, S. G., Godse, P. R., Mulik, R. N., Sen, S., Patil, V. B. (2011) Soft Nanoscience Letters, 01(01): 6–10.
31. Tian, B., Zerbi, G. (1990) J. Chem. Phys., 92(6): 3886–3891.
32. Tian, B., Zerbi, G. (1990) J. Chem. Phys., 92(6): 3892–3898.
33. Sabouraud, G., Sadki, S., Brodie, N. (2000) Chem. Soc. Rev., 29(5): 283–293.
34. Genies, E., Bidan, G., Diaz, A. (1983) J. Electroanal. Chem. Interfacial Electrochem., 149: 101–113.
35. Funt, B. L., Diaz, A. F. (1991) Organic Electrochemistry: an Introduction and a Guide, Marcel Dekker, New York, p. 1337.
36. Mičušík, M., Nedelčev, T., Omastová, M., Krupa, I., Olejníková, K., Fedorko, P., Chehimi, M. M. (2007) Synthetic Met., 157(22–23): 914–923.
37. Hafaid, I., Chebil, S., Korri-Youssoufi, H., Bessueille, F., Errachid, A., Sassi, Z., Ali, Z., Abdelghani, A., Jaffrezic-Renault, N. (2010) Sensor. Actuat. B-Chem., 144: 323–331.
38. Bourigua, S., Hafaid, I., Korri-Youssoufi, H., Maaref, A., Jaffrezic-Renault, N. (2009) Sens. Lett, 7: 731–738.
39. Jaffrezic-Renault, N., Errachid, A. (2011) Biocybern. and Biomed., 31: 3–16.
40. Park, S., Yoo, J. (2003) Analytical Chemistry, 75(21): 455A–461A.
41. Hallik, A., Alumaa, A., Tamm, J., Sammelselg, V., Väärtnõu, M., Jänes, A., Lust, E. (2006) Synthetic Met., 156: 488–494.
42. Halliwell, C. M., Cass, A. E. (2001) Analytical Chemistry, 73(11), 2476–2483.